Proceedings of the ASME 2017 International Mechanical Engineering Congress & Exposition
IMECE 2017
November 3-9, 2017, Tampa, USA

IMECE2017-71515

EFFECT OF THE SPATIAL INHOMOGENEITY OF FRACTURE STRENGTH ON FRACTURE PATTERN FOR QUASI-BRITTLE MATERIALS

Philip L. Clarke*
Mechanical, Aerospace
& Biomedical Engineering Dept.
University of Tennessee Space Institute
411 B.H. Goethert Pkwy.
Tullahoma, Tennessee 37388
Email: pclarke@utsi.edu

Reza Abedi
Bahador Bahmani
Mechanical, Aerospace
& Biomedical Engineering Dept.
University of Tennessee Space Institute
411 B.H. Goethert Pkwy.
Tullahoma, Tennessee 37388

Katherine A. Acton
Sarah C. Baxter
School of Engineering
University of St. Thomas
2115 Summit Ave.
St. Paul, Minnesota 55105

ABSTRACT

The response of quasi-brittle materials is greatly influenced by their microstructural architecture and variations. To model such statistical variability, Statistical Volume Elements (SVEs) are used to derive a scalar fracture strength for domains populated with microcracks. By employing the moving window approach the probability density function and covariance function of the scalar fracture strength field are obtained. The Karhunen-Loève method is used to generate realizations of fracture strength that are consistent with the SVE-derived statistics. The effect of homogenization scheme, through the size of SVE, on fracture pattern is studied by using an asynchronous spacetime discontinuous Galerkin (aSDG) finite element method, where cracks are exactly tracked by the method's adaptive operations.

INTRODUCTION

Due to the lack significant bulk energy dissipative mechanisms for quasi-brittle materials, their mechanical response is greatly influenced by microscale distribution of defects [1]. Size effect, the decrease of fracture strength as the size of a specimen increases, and variations in crack patterns, ultimate loads, *e.g., cf.* [2,3] are some consequences of the high sensitivity of quasi-brittle materials to their microstructural defects. Randomness and inhomogeneity of material is considered in geometry [2–4], initial damage state [5,6], elasticity [7,8], strength [6,9], or fracture toughness and cohesive strength [10,11].

The variability in a material property can be either *explicitly* modeled, by direct modeling of microstructural constituents, *e.g.,* [12–14], or *implicitly.* In implicit approaches phenomenological models, *e.g.,* Weibull model [15], is used as in [16] or macroscopic effective constitutive quantities are derived with a homogenization approach wherein the elemental problem is solved in a thermodynamically consistent *Volume Element* (VE). There are two commonly used classes of VEs known as *Representative Volume Element* (RVE) and *Statistical Volume Elements* (SVEs) [17, 18]. Employing SVEs in random media can be a more accurate averaging approach than utilizing RVEs for two reasons; first, they maintain spatial inhomogeneity of material property which is important in generation of stress concentration and nucleation of cracks from weak sites. Second, due to their statistical nature they can model macroscopic probabilistic variations in ultimate load and fracture energy.

The authors have previously employed implicit approaches based on Weibull model in [16], and SVE homogenization in [19]. We choose an approach similar to the latter work by using SVEs to generate random fields for fracture strength. But, we study the impact of SVE size

*Address all correspondence to this author.

on generated random fields and investigate how they will influence the induced fracture pattern. In addition, unlike the prior work, their is no approximation involved in the Karhunen-Loève (KL) approach by forcing the Probability Density Function (PDF) of the random field to be lognormal. Specifically, we use the CDF-inverse approach to map back and forth between the original statistics of the random fracture field and a standard normal field used for the generation of the KL grid. Finally, the asynchronous Spacetime Discontinuous Galerkin (aSDG) method is used to simulate crack propagation on random fields realized based on different SVE window sizes. As demonstrated, more realistic fracture patterns are obtained for realizations that are based on smaller SVE window sizes.

FORMULATION

In this section we review the derivation of fracture strength, by using SVEs with microcracks, and the generation of statistically consistent grids for fracture strength based on SVE results.

Computation of Fracture Strength for an SVE

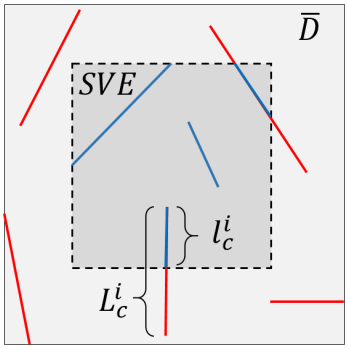

FIGURE 1. CRACKS CONSIDERED FOR COMPUTATION OF EFFECTIVE STRENGTH FOR AN SVE; BULE AND RED COLORS CORRESPOND TO CRACK SEGMENTS INSIDE AND OUTSIDE THE SVE, RESPECTIVELY.

Figure 1 shows a sample SVE in domain $\bar{D}$. The cracks that are fully or partially in the SVE are considered in the computation of its fracture strength $\bar{s}$. The fracture strength is computed by finding the minimum tensile stress, along all directions, such that at least for one of the crack tips in the SVE, $K = K_c$ where K is the stress intensity factor at the crack tip and K_c is the fracture toughness of the given material.

Clearly, the microcrack propagation criterion at the SVE level is assumed to follow the linear elastic fracture mechanics (LEFM) theory. The association of the stress that result in propagation of one SVE with the SVE's fracture strength is motivated by the behavior of quasi-brittle materials where there is a very small difference between the stresses that initiate fracture and the ultimate stress (fracture stress); *cf.* the results in [20]. For our model the point of departure from linear elasticity and initiation of failure corresponds to the stress at which the first microcrack propagates. Finally, instead of doing a full FE analysis, we assume that the stress intensity factor of each crack can be approximated by that of a crack in an infinite domain. While this is still expected to model spatial variation of fracture strength relatively well, in forthcoming works we aim to use FEM analyses for this purpose.

Let L_c and l_c be the original length and length of the ith microcrack within the SVE, respectively. The critical stress for this specific ith microcrack within the SVE is given by the equation

$$\bar{s}^{\,i} = \left(\frac{L_c^i}{l_c^i}\right)^{\alpha} \frac{K_c}{\sqrt{\pi L_c^i/2}}, \tag{1}$$

where as mentioned K_c is the fracture toughness and α is a constant value coefficient. The values of $\alpha = 0$ and $\alpha = \frac{1}{2}$ consider the full length of the crack, L_c^i, and the length of the crack inside the SVE, l_c^i, respectively; accordingly, similar to [19] we choose $\alpha = \frac{1}{4}$ to consider an intermediate length of the crack between L_c^i and l_c^i when it intersects the SVE boundaries. After computing critical stresses $\bar{s}^{\,i}$ for all cracks $i \in \mathcal{I}$, the strength of the SVE $\bar{s}$ is defined as,

$$\bar{s} = min_{i\in\mathcal{I}}\{\bar{s}^{\,i}\}. \tag{2}$$

By this definition, a fracture strength value $\bar{s}$ is assigned to SVEs constructed at all spatial positions and for all random realizations that are generated based on the statistics of microcracks. The point values of $\bar{s}$ are used to compute its probability density function (PDF). The covariance function needed for the Karhunen-Loève method is obtained by the moving technique [21], where the sampling SVE is gradually moved in the domain to determine the trend on which fracture strength changes spatially.

Karhunen-Loeve (KL) Expansion

For a given domain $\bar{D}$ the Karhunen-Loève (KL) method enables generating random fields for a variable ξ, consistent with its underlying statistics, in this case its point-wise PDF and two-point covariance function. The value of the random field ξ is derived based on a random variable ω, that is $\xi = \xi(\mathbf{x}, \omega)$. Having these functions (at all points), it is possible to derive a simple formula which ap-

proximates the mean and covariance of the known random variable distribution; the truncated KL expansion of the random field $\xi = \xi(\mathbf{x},\omega)$ yields the following representation of the field,

$$\xi(\mathbf{x},\omega) = \mu_\xi(\mathbf{x}) + \sum_{i=1}^{n_{KL}} \sqrt{\lambda_i} b_i(\mathbf{x}) Y_i(\omega) \tag{3}$$

where $\{\lambda_i, b_i(\mathbf{x})\}_{i=1}^{n_{KL}}$ are eigen-pairs determined from the covariance of the random field and $Y_i(\omega)$ are centered, uncorrelated random variables [1] which derive the probability distribution of the random field. For an arbitrary PDF function for $\xi(\mathbf{x},\omega)$, Y_i are only uncorrelated. To make this formula practical and be able to generate random variables Y_i *independent* of each other, they should be independent random variables. The latter condition holds if $\xi(\mathbf{x},\omega)$ is point-wise Gaussian. Thus, Eqn. (3) is to be used for a normal field. In our prior work [19], we approximated the fracture strength field by a lognormal field to be able to directly use Eqn. (3) on $\log(\bar{s})$. However, in general we need to transfer a random field ξ to η, a random field with point-wise Gaussian distribution before using the KL method. Then a random field for the mapped normal field η is generated, and finally the random field is transferred back to its original form. The KL expansion for the Gaussian random field $\eta(\mathbf{x},\omega) \sim N(\mu_\eta, \sigma_\eta)$ is,

$$\eta(\mathbf{x},\omega) = \mu_\eta(\mathbf{x}) + \sum_{i=1}^{n_{KL}} \sqrt{\lambda_i} b_i(\mathbf{x}) y_i, \tag{4}$$

where μ_η and σ_η are the mean value and standard deviation of η. The aforementioned eigen-pairs of the spatial eigenfunctions $b_i(\mathbf{x})$ and eigenvalues λ_i are obtained by solving a generalized eigenvalue problem (EVP) that can be solved by finite element method (FEM) discretization; *cf.* [22].

As mentioned, a general non-Gaussian random field $\xi(\mathbf{x},\omega)$ is first mapped to a Gaussian random field $\eta(\mathbf{x},\omega)$. This map is expressed through the *Inverse Transformation Method*,

$$\eta(\mathbf{x},\omega) = F_\eta^{-1}(F_\xi(\xi(\mathbf{x},\omega))), \tag{5}$$

where F_ξ and F_η are the Cumulative Density Functions (CDF) of the non-Gaussian and Gaussian random fields, respectively. We use a standard normal, *i.e.,* $\mu_\eta = 0$ and $\sigma_\eta = 1$, for the Gaussian field. Finally, for any of the random field realizations of η, obtained by Eqn. (4), we use the inverse of the map in Eqn. (5) to transfer it back to ξ. This transformation for ξ (equal to fracture strength $\bar{s}$) is expressed as,

$$\bar{s}(\mathbf{x}) = \xi(\mathbf{x}) = F_\xi^{-1}\Big(\frac{1}{2}\big[1 + \mathrm{Erf}\Big(\frac{\eta(\mathbf{x})}{\sqrt{2}}\Big)\big]\Big). \tag{6}$$

This is a more accurate extension of [19] wherein the original field $\xi(\mathbf{x},\omega)$ and CDF F_ξ assumed a Log-normal probability distribution. We note that the covariance function for $\eta(\mathbf{x},\omega)$, which is required in solving the KL eigen-problem, is characterized by a moving window approach; *cf.* [19] for more details.

NUMERICAL RESULTS

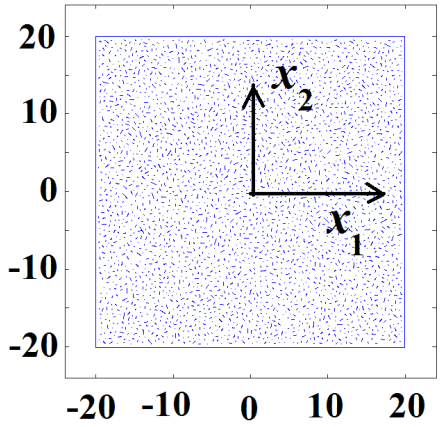

(a) EXAMPLE OF REALIZATION $\bar{D}$ WITH RANDOM MICROSTRUCTURE ARCHITECTURE.

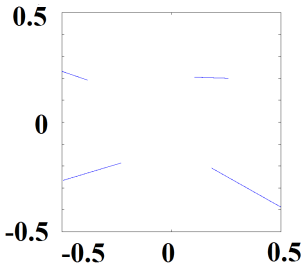

(b) SVE ($L_{VE} = 1$) SAMPLE FROM Fig. 2a CENTERED AT $\mathbf{x} = (0,0)$.

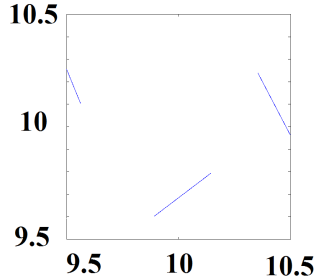

(c) SVE ($L_{VE} = 1$) SAMPLE FROM Fig. 2a CENTERED AT $\mathbf{x} = (10,10)$.

FIGURE 2. A 40 mm × 40 mm DOMAIN AND TWO SAMPLED SVES.

[1] $\mathbb{E}(Y_i(\omega)) = 0$, and $\mathbb{E}(Y_i(\omega)Y_j(\omega)) = 0$

The spatial domain $\bar{D}$ used for generating the following statistical data is a simple rectangular domain centered at the Cartesian position $\mathbf{x}_{center} = (0,0)$ and spanning 40 length units ($L_{\bar{D}} = 40$ mm) in both $\mathbf{e}_1$ and $\mathbf{e}_2$ directions.

To generate domain microstructural realizations with microcracks, we assume that the microcrack length follows a Weibull distribution [15, 23] and its angle a uniform distributed between $[0\ 2\pi]$. Furthermore, the average and standard deviation of microcrack length are 330 μm and 170 μm, respectively. Finally, we use a take-and-place algorithm to distribute generated cracks within domain $\bar{D}$. A sample realization is shown in Fig. 2a. Two sample SVEs generated from the domain in Fig. 2a are shown in Fig. 2b and Fig. 2c. The center points of sampled SVEs form a nonuniform grid, with a denser spacing near zero distance, to have a more accurate derivation of covariance function.

The effect of the SVE size on random field statistics

The size of the SVE directly influences the statistics of the random field characterized. To study the relation between the SVE size and the fracture strength random field statistics, square SVEs with edge sizes of 1, 2, 4, 8 and 16 mm were considered. The PDFs of the fracture strength field in Fig. 3 are accordingly labeled by SVE$\mathbf{1}\times\mathbf{1}$, SVE$\mathbf{2}\times\mathbf{2}$, SVE$\mathbf{4}\times\mathbf{4}$, SVE$\mathbf{8}\times\mathbf{8}$, and SVE$\mathbf{16}\times\mathbf{16}$.

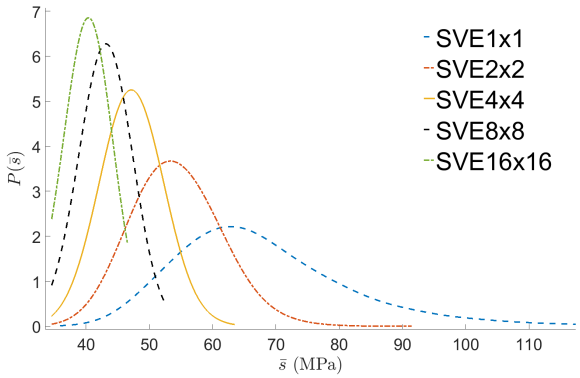

FIGURE 3. THE EFFECT OF THE SVE SIZE ON THE PDF OF RANDOM FIELD $\bar{s}$.

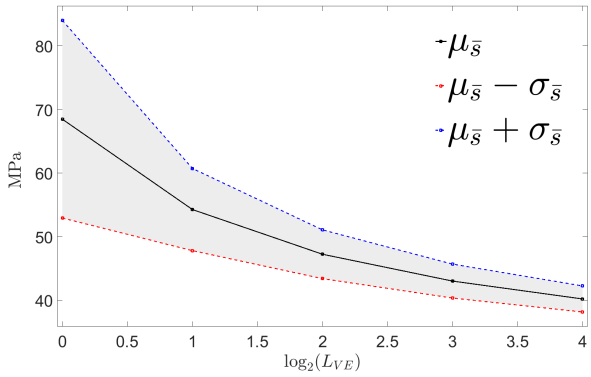

FIGURE 4. THE EFFECT OF THE SVE SIZE ON RANDOM FIELD $\bar{s}$ STATISTICS.

As the SVE size becomes larger, the peek of the PDF curve shifts to the left, that is a weaker material is represented. This is the well-known size effect for quasi-brittle materials; as the size of the domain increases there is a larger likelihood that a more critical crack or defect exists in it. That is why larger samples tend to have lower fracture strengths. In fact, domain size calibrated Weibull model and many other stochastic models in the literature attempt to represent this phenomenon.

Another observation is that as the window size decreases, the sampled fracture strength values are more likely to have wider variations. The reason is that at small sizes, the SVE may land in a region with long crack(s) or a short one, thus yielding a low or a high fracture strength, respectively. This is demonstrated by higher standard deviations for smaller SVE window sizes in Fig. 4. On the contrary, as the SVE window size increases, the standard deviation decreases, *i.e.,* PDF function becomes narrower. This is expected, because as the window size increases many defects (microcracks) are included in the SVE and all SVEs tend to have roughly the same critical crack length.

KL random fields

The KL random field meshes were generated based on the assumption that the material modeled was isotropic with a rotationally invariant scalar fracture strength, and the covariance function depending only on distance between two arbitrary points. Moreover, the covariance function for fracture strength—casted to a standard normal Gaussian distribution, *cf.* η in Eqn. (5)—is interpolated by the exponentially decaying function,

$$COV(\eta(\mathbf{x}^1),\eta(\mathbf{x}^2)) = e^{-\left(\frac{|\mathbf{x}^1-\mathbf{x}^2|}{d_c}\right)^2}, \qquad (7)$$

where d_c is a characteristic correlation length scale implied by the form of the function. It is noted that, the exponential function from Eqn. (7) is a very good fit for the numerically obtained covariance functions. The correlation lengths for different SVE sizes are $d_c^{1\times1} = 0.52$ mm, $d_c^{2\times2} = 0.96$ mm, $d_c^{4\times4} = 1.84$ mm, $d_c^{8\times8} = 3.98$ mm, and $d_c^{16\times16} = 8.19$ mm respectively, and their covariance functions are shown in Fig. 5. To ensure that accurate KL grids are constructed, enough number of terms should be considered in Eqn. (3) so that last eigenvalues are very close to zero; for the SVE1×1 sampling, at $n_{KL} \approx 1500$ eigenvalues are extremely close to zero, and even fewer terms are needed for larger sampling window sizes. For all the KL grids generated subsequently, $n_{KL} = 2000$ eigenvalues / eigenvectors are considered.

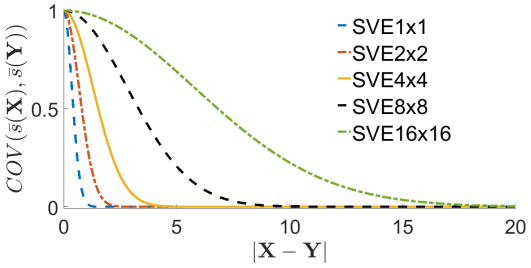

FIGURE 5. ONE-DIMENSIONAL COVARIANCE FUNCTIONS BASED ON VARIABLE SVE SIZES.

Discrete grids for fracture strength and FEM solution

We use two different discrete grids for our fracture simulations. The *material grid* is used for the generation and storage of fracture strength and the *aSDG spatial grid* is the finite element discrete mesh used for fracture simulation. The former is a uniform grid on which the KL eigenvalue problem is solved; *cf.* the formulation section and [22]. The latter is used for the solution of dynamic fracture problem, which is nonuniform. Adaptive operations are used to control solution discretization error and accommodate arbitrary oriented crack paths. For fracture simulations in this manuscript a 16mm $\times$ 16mm domain is considered. Note that this domain is different from the 40mm $\times$ 40mm domains used in Fig. 2a. In the latter case, domains with micro-structure (microcracks herein) are generated to derive the first and second moments needed for the KL method, while in the former case the KL grids are generated based on such derived statistics. It should be noted that the sizes of these domains do not need to be the same. Finally, the KL domains generated subsequently do not include any microcracks, as the effect of microcracks is already incorporated in the inhomogeneous and randomly sampled fracture strength field.

Accordingly, a structured 2D mesh of dimensions $[-8,8]$ mm $\times$ $[-8,8]$ mm is used for the KL expansion method. For this grid, 2D quadrilateral elements (60×60 elements) of equal element size are used for solving the eigenvalue problem and generating random field realizations. The KL discretization mesh is shown in Fig. 6.

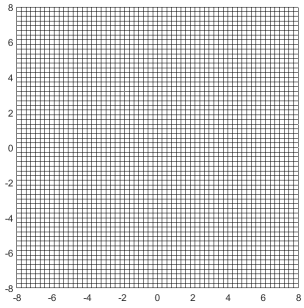

FIGURE 6. STRUCTURED MESH FOR KL EIGENVALUE PROBLEM AND RANDOM FIELD REALIZATIONS.

One KL random field realization for fracture strength $\bar{s}$ for each of the available SVE sizes is depicted in Fig. 7. The decrease of each SVE size yielded a greater variability in fracture strength randomness within a given length-scale; this behavior agrees with theoretical expectations of how SVE sizes affect random field value scatter.

Dynamic fracture under uniform uniaxial applied tensile stress

We use an h-adaptive asynchronous spacetime discontinuous Galerkin (aSDG) finite element method [24, 25] for our dynamic fracture simulations. The aSDG method directly discretizes spacetime using nonuniform grids that satisfy a special causality constraint [26] yielding unique properties such as local and asynchronous solution scheme, arbitrarily high and local temporal order of accuracy, and linear solution scaling with number of elements. This numerical scheme, implemented in C++, utilizes the aforementioned features as well as advanced adaptive operations in spacetime to very accurately and efficiently capture complex fracture patterns by a *crack tracking* adaptive scheme [27, 28]. The solution is mesh independent and accommodates crack propagation in any desired direction, a feature similar to the popular XFEM and GFEM methods, but removes the need to enrich element basis functions. All these features make the aSDG method ideal for dynamic quasi-brittle fracture simulations reported herein.

This section aims to validate the method's ability to capture fracture nucleation at domain locations of weaker fracture strength as well as track the development of a possibly complex crack network. The FEM domain is a 2D quadrilateral of side length 8 centered are $\mathbf{x} = (0,0)$. The bulk material properties are: Young's Modulus $E =$

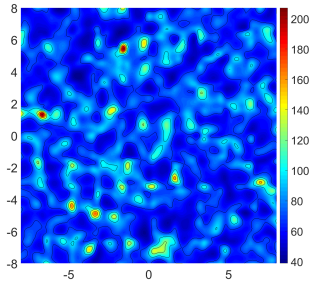

(a) RANDOM $\bar{s}$ FIELD FOR SVE1 $\times$ 1

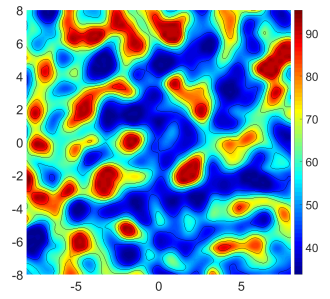

(b) RANDOM $\bar{s}$ FIELD FOR SVE2 $\times$ 2

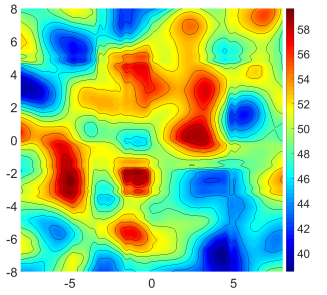

(c) RANDOM $\bar{s}$ FIELD FOR SVE4 $\times$ 4

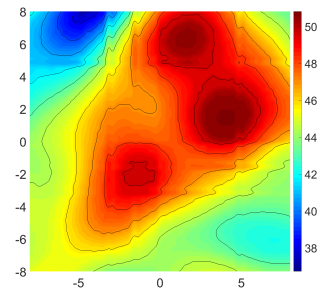

(d) RANDOM $\bar{s}$ FIELD FOR SVE8 $\times$ 8

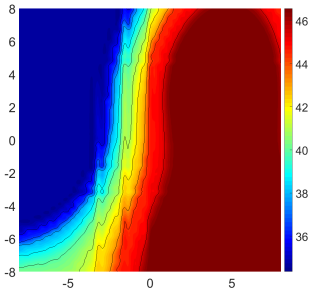

(e) RANDOM $\bar{s}$ FIELD FOR SVE16 $\times$ 16

FIGURE 7. THE FIRST REALIZATION OF KL-GENERATED RANDOM FIELD MESHES FOR FRACTURE STRENGTH $\bar{s}$ (in MPa) WITH RESPECT TO DIFFERENT SVE SIZES.

3.24 GPa, mass density $\rho = 1190\ kg/\mathrm{m}^3$, and Poisson's ratio $\nu = 0.35$. The values of fracture strength $\bar{s}(\mathbf{x})$ are extracted from the independent KL random field solution discretization. The fracture strength equation parameters used in the SVE sampling algorithm are fracture toughness $K_c = 1.5\mathrm{MPa}\sqrt{m}$ and coefficient $\alpha = \frac{1}{4}$. The initial and boundary conditions are specified consistent with displacement field $\mathbf{u}(\vec{x},t) = (u_1(\vec{x},t),\ u_2(\vec{x},t)) = (ax_1t,\ 0.0)$ where $a > 0$ and $(\mathbf{x},t)$ is the spacetime coordinate of a point. This corresponds to a spatially uniform stress field in x_1 direction, a condition that will no longer hold after the nucleation/propagation of the first crack. As will be discussed below, this uniform stress field very well demonstrates the shortcoming of models that use a spatially constant fracture strength. For the following results, the value of $a = 1.062/\mathrm{ms}$ is chosen.

Comparative study: random vs homogeneous fracture strength fields To understand the effect of incorporating randomness into a fracture model of quasi-brittle material, fracture solutions generated from the use of a spatially *homogeneous* fracture strength field is compared to solutions which facilitate KL-generated random fracture strengths. Specifically, the first KL mesh realizations for 1×1 and 8×8 SVEs are used for nonuniform fields for $\bar{s}$; *cf.* Figures 7a and 7d.

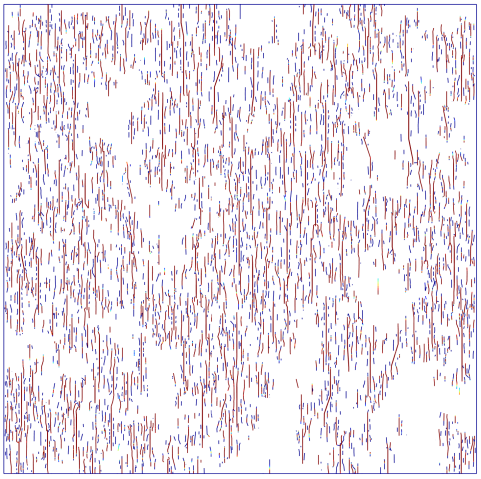

FIGURE 10. HOMOGENEOUS SOLUTION DEFORMED SHAPE AT TIME, $t \approx 3.9\ \mu$s.

We first study the development of the SVE1 $\times$ 1 fracture network to demonstrate how the variability of the fracture strength influences random nucleation locations as well as fracture patterns characteristics. Figure 8 shows the visualization of intermediate fracture solutions on deformed geometry. The color and height fields correspond to strain and kinetic energy densities, respectively. As the solution time progresses a clear correlation between the fracture strength distribution and the site of fracture nucleation is demonstrated; *cf.* Figure 7a. As the boundary loading increases cracks accelerate and characteristics of brittle fracture such as microcracks / crack bifurcations are observed.

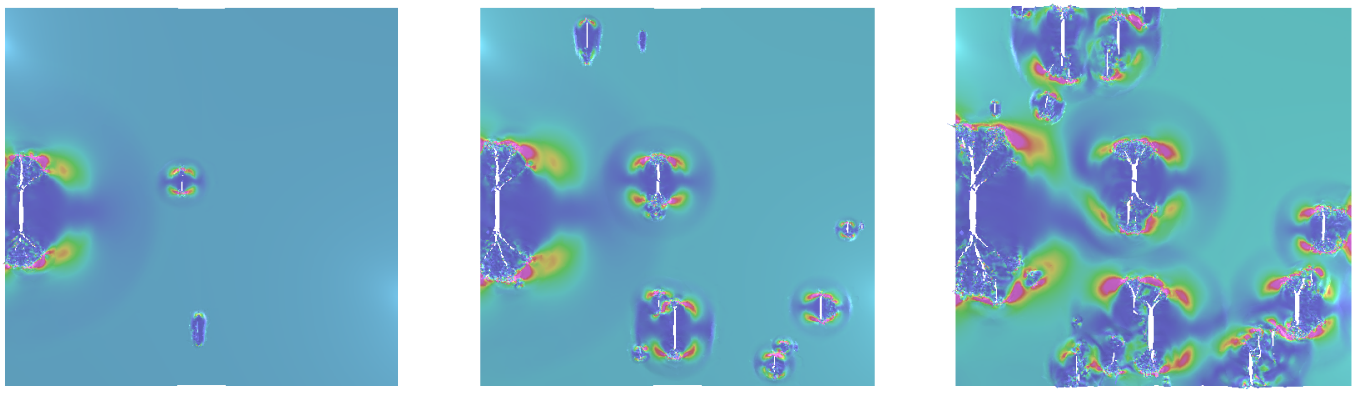

(a) TIME $t = 7.250$ μs. (b) TIME $t = 7.875$ μs. (c) TIME $t = 8.625$ μs.

FIGURE 8. A SEQUENCE OF FRACTURE SOLUTION VISUALIZATIONS FOR SVE1 $\times$ 1 mm.

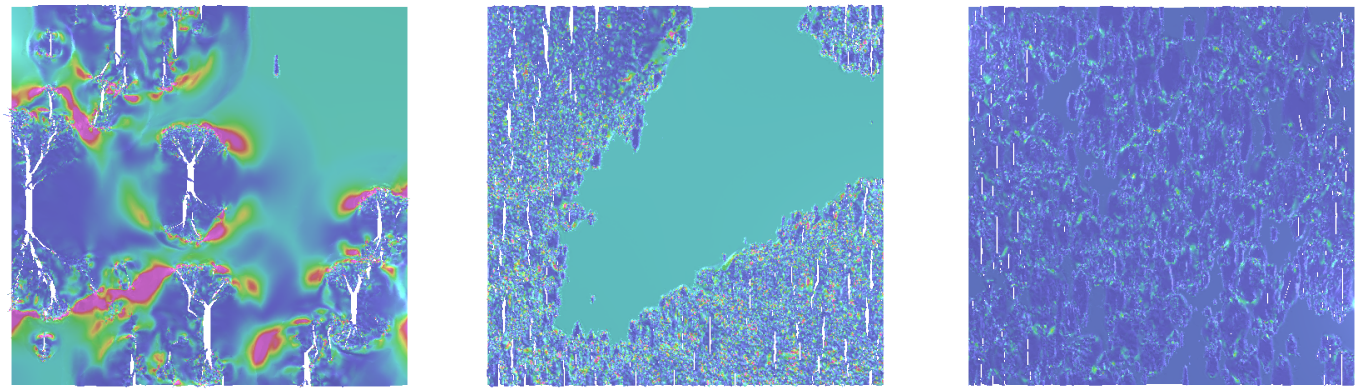

(a) SVE1 $\times$ 1, TIME $t = 9.25$ μs. (b) SVE8 $\times$ 8, TIME, $t = 8.65$ μs. (c) HOMOGENEOUS $\bar{s}$, TIME $t = 3.9$ μs.

FIGURE 9. FRACTURE SOLUTION VISUALIZATION WITH VARYING FRACTURE STRENGTH RANDOMNESS.

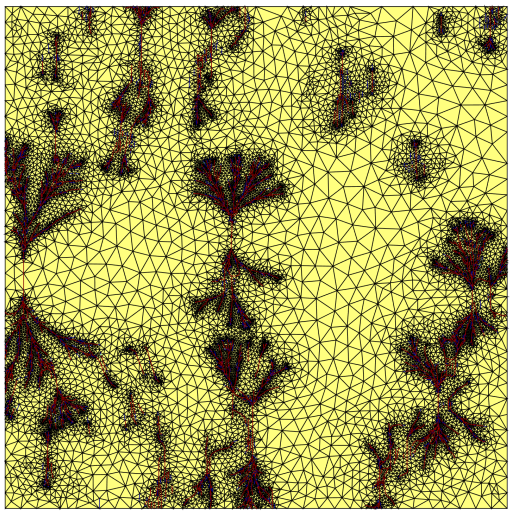

FIGURE 11. SVE1 $\times$ 1 SOLUTION DISCRETIZATION AT TIME, $t \approx 9.648$ μs.

In Figure 9 the effect of SVE sampling window size, and consequently correlation length scale, on developed fracture patterns is studied. As the sve size increases, there is a decrease in the degree of spatial variation of the strength values and potentially larger areas of weaker strength. Fractures based on 1×1 mm SVE homogenization in Fig. 9a are closer to what is expected from brittle fracture by forming distinct cracks with microcracking and crack branching events. The solution for 8×8 mm SVE homogenization are shown in Fig. 9b; as can be seen there is an excellent agreement between regions with fracture and those with lower fracture strength $\bar{s}$ from the first realization used in Fig. 7d. Within these large weaker areas with almost the same fracture strength, greater number of nucleation sites occur resulting in clusters of relatively smaller cracks. Finally, Fig. 9c demonstrates fracture pattern predicted when a homogeneous fracture strength is used for the entire domain; the fracture network can be better seen in Fig. 10, where the deformed solution geometry represented by linear segments is color–coded based on a scalar damage value (blue segments are undamaged and red segments are beyond a critical damage value). The fracture network is densely populated compared to the SVE1 $\times$ 1 case; also, since the domain contains no variation in fracture strength value, the location of these fracture sites is merely based on numeri-

cal errors in the FEM solution rather than microstructure variations.

The importance of mesh adaptivity is demonstrated in Fig. 11 for SVE1 $\times$ 1 results, where crack segments are represented by red 2D line segments in the space front; adaptive operations enable exact tracking of crack direction and accurate resolution of fracture process zone size.

CONCLUSION

SVEs and the moving window approach were used to derive the statistics of a scalar fracture strength field for domains with random distribution of microcracks. The Inverse Transform Method was used to transform the derived non-Gaussian random field to a standard normal field to enable the generation of statistically consistent random fields with the Karhunen-Loève method, and to transfer the generated random field back to its non-Gaussian form. The fracture simulations, obtained by the aSDG method, demonstrated the effect of the size of SVE on fracture formation where microcracking, crack branching and other features of brittle fracture were more evident with smaller SVE sizes.

ACKNOWLEDGMENT

The authors gratefully acknowledge partial support for this work via the U.S. National Science Foundation (NSF), CMMI - Mechanics of Materials and Structures (MoMS) program grant numbers 1538332 and 1654198.

REFERENCES

[1] Genet, M., Couegnat, G., Tomsia, A., and Ritchie, R., 2014. "Scaling strength distributions in quasi-brittle materials from micro- to macro-scales: A computational approach to modeling nature-inspired structural ceramics". *Journal of the Mechanics and Physics of Solids,* ***68***(1), pp. 93–106.

[2] Al-Ostaz, A., and Jasiuk, I., 1997. "Crack initiation and propagation in materials with randomly distributed holes". *Engineering Fracture Mechanics,* ***58***(5-6), pp. 395–420.

[3] Sobczyk, K., 2008. "Morphological complexity of material microstructures: From stochastic models to fracture estimation". *Probabilistic Engineering Mechanics,* ***23***(4), pp. 444–455.

[4] Wriggers, P., and Moftah, S., 2006. "Mesoscale models for concrete: Homogenisation and damage behaviour". *Finite Elements in Analysis and Design,* ***42***(7), pp. 623–636.

[5] Hassold, G., and Srolovitz, D., 1989. "Brittle fracture in materials with random defects". *Physical Review B (Condensed Matter),* ***39***(13), pp. 9273–9281.

[6] Carmeliet, J., and Hens, H., 1994. "Probabilistic nonlocal damage model for continua with random field properties". *Journal of Engineering Mechanics,* ***120***(10), pp. 2013–2027.

[7] Cox, S., and Paterson, L., 1989. "Tensile fracture of heterogeneous solids with distributed breaking strengths". *Physical Review B (Condensed Matter),* ***40***(7A), pp. 4690–4695.

[8] Dimas, L., Giesa, T., and Buehler, M., 2014. "Coupled continuum and discrete analysis of random heterogeneous materials: Elasticity and fracture". *Journal of the Mechanics and Physics of Solids,* ***63***(1), pp. 481–490.

[9] Levy, S., and Molinari, J., 2010. "Dynamic fragmentation of ceramics, signature of defects and scaling of fragment sizes". *Journal of the Mechanics and Physics of Solids,* ***58***(1), pp. 12–26.

[10] Curtin, W., 1997. "Toughening in disordered brittle materials". *Physical Review B-Condensed Matter,* ***55***(17), pp. 11270–11276.

[11] Shanmugam, V., Penmetsa, R., Tuegel, E., and Clay, S., 2013. "Stochastic modeling of delamination growth in unidirectional composite DCB specimens using cohesive zone models". *Composite Structures,* ***102***, pp. 38–60.

[12] Schlangen, E., and Garboczi, E., 1997. "Fracture simulations of concrete using lattice models: computational aspects". *Engineering Fracture Mechanics,* ***57***(2-3), pp. 319–332.

[13] Li, J., 2000. "Debonding of the interface as 'crack arrestor"'. *International Journal of Fracture,* ***105***(1), pp. 57–79.

[14] Abedi, R., Omidi, O., and Clarke, P., 2016. "Numerical simulation of rock dynamic fracturing and failure including microscale material randomness". *Proceeding: 50th US Rock Mechanics/Geomechanics Symposium, June 26-June 29, Houston, Texas - USA*, pp. ARMA 16–0531 (13 pages).

[15] Weibull, W., 1939. "A statistical theory of the strength of materials". *R. Swed. Inst. Eng. Res.*, p. Res. 151.

[16] Abedi, R., Omidi, O., and Clarke, P., 2017. "A numerical study on the effect of loading and randomness on fracture patterns in a tight formation". *Proceeding: 51th US Rock Mechanics/Geomechanics Symposium, June 25-June 28, San Francisco, California USA*, pp. ARMA 17–0641 (12 pages).

[17] Tregger, N., Corr, D., Graham-Brady, L., and Shah, S., 2006. "Modeling the effect of mesoscale randomness on concrete fracture". *Probabilistic Engineering Mechanics,* ***21***(3), pp. 217–225.

[18] Segurado, J., and LLorca, J., 2006. "Computational micromechanics of composites: The effect of particle spatial distribution". *Mechanics of Materials,* ***38***(8-10), pp. 873–883.

[19] Clarke, P., and Abedi, R., 2017. "Fracture modeling of rocks based on random field generation and simulation of inhomogeneous domains". *Proceeding: 51th US Rock Mechanics/Geomechanics Symposium, June 25-June 28, San Francisco, California USA*, pp. ARMA 17–0643.

[20] Nguyen, V. P., Lloberas-Valls, O., Stroeven, M., and Sluys, L. J., 2011. "Homogenization-based multiscale crack modelling: From micro-diffusive damage to macro-cracks". *Computer Methods in Applied Mechanics and Engineering,* ***200***(9), pp. 1220–36.

[21] Baxter, S., and Graham, L., 2000. "Characterization of random composites using moving-window technique". *Journal of Engineering Mechanics,* ***126***(4), pp. 389–397.

[22] Ghanem, R., and Spanos, P., 1991. *Stochastic finite elements: a spectral approach*. Springer-Verlag.

[23] Weibull, W., 1951. "A statistical distribution function of wide applicability". *Journal of Applied Mechanics,* ***18***, pp. 293–297.

[24] Abedi, R., Haber, R. B., and Petracovici, B., 2006. "A spacetime discontinuous Galerkin method for elastodynamics with element-level balance of linear momentum". *Computer Methods in Applied Mechanics and Engineering,* ***195***, pp. 3247–3273.

[25] Abedi, R., Haber, R. B., Thite, S., and Erickson, J., 2006. "An *h*–adaptive spacetime–discontinuous Galerkin method for linearized elastodynamics". *Revue Européenne de Mécanique Numérique (European Journal of Computational Mechanics),* ***15***(6), pp. 619–642.

[26] Abedi, R., Chung, S.-H., Erickson, J., Fan, Y., Garland, M., Guoy, D., Haber, R., Sullivan, J. M., Thite, S., and Zhou, Y., 2004. "Spacetime meshing with adaptive refinement and coarsening". In Proceedings of the Twentieth Annual Symposium on Computational Geometry, SCG '04, ACM, pp. 300–309.

[27] Abedi, R., 2010. "Spacetime damage-based cohesive model for elastodynamic fracture with dynamic contact". PhD thesis, Department of Theoretical and Applied Mechanics, University of Illinois at Urbana–Champaign.

[28] Omidi, O., Abedi, R., and Enayatpour, S., 2015. "An adaptive meshing approach to capture hydraulic fracturing". *The 49th US Rock Mechanics/Geomechanics Symposium, June 28-July 1, San Francisco,CA,USA*(ARMA 15-572).